IAC–21–C1.5.5

Round-Trip Trajectories Between Earth-Moon NRHOs and Heliocentric Space in the Earth-Moon-Sun System

Kenza K. Boudad
Purdue University, USA, kboudad@purdue.edu

Kathleen C. Howell
Purdue University, USA, howell@purdue.edu

Diane C. Davis
a.i.solutions, Inc., USA, diane.davis@ai-solutions.com

In the next decades, multiple missions are proposed or planned that originate in the vicinity of the Moon with the expected delivery of a spacecraft to heliocentric space, e.g., servicing missions to the Nancy Roman or the James Webb Space Telescopes, as well as departures from Gateway to other interplanetary destinations. The Earth-Moon-Sun transit dynamics are complex, primarily influenced by the Earth and the Moon in cislunar space; the gravitational influence of the Sun becomes significant after departure from the Earth-Moon vicinity. The current investigation leverages dynamical structures in the BCR4BP such as periodic orbits and manifolds, to design low-energy, round-trip transfers between the cislunar and heliocentric spaces.

I. Introduction

Transit between the lunar vicinity and the region near the Sun-Earth libration points presents many interesting opportunities in the near future. The NASA Gateway facility is the current framework for the development of a hub near the Moon with an option to return to the Lunar surface. From a baseline orbit in an Earth-Moon L_2 Near Rectilinear Halo Orbit (NRHO), the Gateway is intended to serve as a proving ground for deep space technologies and a staging location for missions beyond the cislunar space, as well as a potential transit facility for sample returns before return to Earth. Possible destinations for sample return missions include heliocentric space; for example, various science interests exist at the Sun-Earth L_1 libration point, including the collection of solar wind particles.

In this investigation, sample return transfer trajectories to a heliocentric libration point orbit (LPO) via the Gateway facility are designed within the context of the Bicircular Restricted 4-Body Problem (BCR4BP). The BCR4BP is a time-dependent, periodic model that incorporates the gravitational influences of the Earth, the Moon, and the Sun, acting on a spacecraft. Transfer design within the BCR4BP blends natural flow from both the Earth-Moon and the Sun-Earth systems. One advantage of the BCR4BP is that relevant information concerning the trajectory is available in two frames: the Earth-Moon rotating frame and the Sun-Earth rotating frame. Yet, the BCR4BP avoids the added complexity of the higher-fidelity force model while the dynamics of the Earth-Moon-Sun system are described relatively accurately.

This investigation demonstrates a framework for designing trajectories in a dynamical environment that includes the Earth, the Moon, and the Sun. A sample-return mission scenario is introduced. First, a spacecraft departs the NRHO and transits to a Sun-Earth halo orbit. After two years in the Sun-Earth libration point orbit, the spacecraft returns to the NRHO. The methodology is effective for transit between any cislunar orbit and the Sun-Earth libration point regions; the framework demonstrates its capability employing the NRHOs, which possess complex cislunar dynamics and near-stable properties. Challenges in the trajectory design process include the phasing of the trajectory with respect to the Earth, the Moon, the Sun, and the Gateway platform. Various geometries for transfers are presented, and their associated times of flight and energy characteristics are observed.

II. Dynamical Models

Two dynamical models are employed in this investigation. The Circular Restricted Three-Body Problem (CR3BP) [1] is an autonomous model approximating the Earth-Moon system dynamics. The Bicir-

cular Restricted Four-Body Problem (BCR4BP)[2–4] is a time-dependent, periodic model describing the motion of a particle in the Earth-Moon-Sun regime. The BCR4BP is an intermediate step between the CR3BP and a higher-fidelity, time-dependent, non-periodic ephemeris model.

II.i The Circular Restricted 3-Body Problem

In the CR3BP, the motion of a spacecraft of negligible mass is subject to the influence of two primary gravitational bodies, for example, the Earth and the Moon. The model assumes that the two primaries are point masses in circular orbits about their common center of mass. The motion of the spacecraft under the influence of the two primaries is described relative to a rotating frame moving at a fixed rate consistent with the circular rotation of the primaries. By convention, the differential equations governing the CR3BP are nondimensionalized. The characteristic quantities employed include: (i) the Earth-Moon distance; (ii) the sum of the primary masses; (iii) a characteristic time such that the nondimensional gravitational constant $\tilde{G}$ equals unity. The nondimensional equations of motion are then

$$\ddot{x} = 2\dot{y} + \frac{\partial U^*}{\partial x}, \quad \ddot{y} = -2\dot{x} + \frac{\partial U^*}{\partial y}, \quad \ddot{z} = \frac{\partial U^*}{\partial z} \quad [1]$$

where x, y, z (respectively, $\dot{x}, \dot{y}, \dot{z}$) are the position (respectively, the velocity) components of the spacecraft expressed in the Earth-Moon rotating coordinates and derivatives as viewed by an observer in the rotating frame. The associated pseudo-potential function U^* is defined as

$$U^* = \frac{1}{2}(x^2 + y^2) + \frac{\mu}{r_{\text{e-sc}}} + \frac{1-\mu}{r_{\text{m-sc}}} \quad [2]$$

The quantities $r_{\text{e-sc}}$ and $r_{\text{m-sc}}$ are the distances between the spacecraft and the primaries, and $\mu = {m_{\text{m}}}/{(m_{\text{e}}+m_{\text{m}})}$ is the mass parameter for the Earth-Moon CR3BP system.

The equations of motion in the CR3BP do not admit a closed-form solution. However, five equilibrium solutions, the libration points, exist and are denoted L_1 through L_5. Stable and unstable orbits in families, such as the L_2 halo orbit family, exist in the CR3BP. The CR3BP allows a single integral of the motion, the Jacobi constant, evaluated as

$$C = 2U^* - \left(\dot{x}^2 + \dot{y}^2 + \dot{z}^2\right) \quad [3]$$

This energy-like quantity limits the motion of the spacecraft to regions where the magnitude of the rotating velocity is real and not a complex quantity. These regions are bounded by Zero Velocity Surfaces (ZVSs). For values of the Jacobi constant greater than the one associated with the L_1 libration point, the ZVSs form two closed regions around each of the primaries. As the energy along the spacecraft trajectory increases, the value of the Jacobi constant decreases until, at the L_1 value, the ZVSs open at the L_1 libration point, and the spacecraft is able to move from the vicinity of one primary to the vicinity of the other. Similarly, when the value of the Jacobi constant decreases to the value associated with L_2, the ZVSs open at L_2 allowing escape beyond the vicinity of the primaries entirely. Thus, the Jacobi constant is an energy-like quantity that bounds motion in the CR3BP.

Orbits of interest in this investigation include the Earth-Moon NRHO subset and the Sun-B_1, that is the Sun-{Earth+Moon} halo orbit families of periodic orbits. The L_1, L_2, and L_3 halo families are comprised of three-dimensional periodic orbits in the CR3BP. The halo family of orbits bifurcate from each family of planar Lyapunov orbits associated with the collinear libration points. The halo orbits are mirrored across the x-y plane: a northern family member possesses a positive z component over the majority of each orbit, while the southern family members are defined by negative z components. The NRHOs are a subset of orbits in the Earth-Moon CR3BP halo families. Zimovan et al.[5] define bounds in the Earth-Moon L_1 and L_2 halo families to define the NRHOs by their linear stability properties. For a spacecraft in one of the selected NRHOs, the CR3BP is a good approximation for the behavior of the trajectory.

II.ii The Bicircular Restricted 4-Body Problem

In scenarios where the gravitational influence of the Sun is non-negligible, a higher-fidelity model is necessary to accurately describe the spacecraft behavior. The BCR4BP incorporates the gravitational effect of three massive bodies, for instance, the Earth, the Moon and the Sun, on the motion of a spacecraft[2–4]. The mass of the spacecraft is assumed to be negligible in comparison to the masses of the other bodies. In this model, the Earth and the Moon are assumed to move in circular orbits around their common barycenter, denoted B_1, while the Sun and B_1 move in circular orbits with respect to the Earth-Moon-Sun barycenter, labeled B_2, as denoted in Fig. 1. The BCR4BP is not a coherent model: the perturbing acceleration from the Sun does not influence the motion of the Earth and the Moon, thus, the motion of the Moon is not a solution to the Sun-

Earth CR3BP. Coherent bicircular models have been investigated previously[3], but are not necessary in this analysis. The equations of motion in the CR3BP, in Eq. (1), are extended to include the solar gravitational influence as follows,

$$\ddot{x} = 2\dot{y} + \frac{\partial \Upsilon^*}{\partial x}, \quad \ddot{y} = -2\dot{x} + \frac{\partial \Upsilon^*}{\partial y}, \quad \ddot{z} = \frac{\partial \Upsilon^*}{\partial z} \quad [4]$$

where Υ^* is the pseudo-potential function in the BCR4BP and evaluated as

$$\Upsilon^* = U^* + \frac{\mu_\mathrm{s}}{r_{\text{s-sc}}} - \frac{\mu_\mathrm{s}}{a_\mathrm{s}^3}(x_\mathrm{s}x + y_\mathrm{s}y + z_\mathrm{s}z) \quad [5]$$

Then, $\mu_\mathrm{s} = \frac{m_\mathrm{s}}{m_\mathrm{e}+m_\mathrm{m}}$ is the nondimensional mass of the Sun and $a_\mathrm{s} = \frac{r_\mathrm{s}}{r_{\text{e-m}}}$ is the nondimensional distance between the Earth-Moon barycenter and the Sun. Note that this adaptation of the BCR4BP assumes the Sun moves in the Earth-Moon plane of motion. The Earth-Moon and Sun-B_1 systems can be modeled in different planes[4], but a planar model suffices for this application. The variables $x_\mathrm{s}, y_\mathrm{s}, z_\mathrm{s}$ are the position components of the Sun, originating at B_1, and expressed in terms of the Earth-Moon rotating frame,

$$\begin{bmatrix} x_\mathrm{s} \\ y_\mathrm{s} \\ z_\mathrm{s} \end{bmatrix} = a_\mathrm{s} \begin{bmatrix} \cos(\theta) \\ \sin(\theta) \\ 0 \end{bmatrix} = \begin{bmatrix} \cos(-\omega\ t + \theta_0) \\ \sin(-\omega\ t + \theta_0) \\ 0 \end{bmatrix} \quad [6]$$

where the Sun angle θ is measured from the rotating $\hat{x}$ axis to the Sun position vector as defined in Fig. 1, and $\omega = 0.9253$ is the magnitude of the nondimensional angular velocity of the Sun as viewed in the Earth-Moon rotating frame. This angular velocity is computed as the difference between the nondimensional mean motion of the Sun in the inertial frame centered at the Earth-Moon barycenter, that is, $n_S = \sqrt{(1+\mu_\mathrm{s})/a_\mathrm{s}^3}$, and the nondimensional mean motion of the Earth-Moon system with respect to the same observer, n, that is, the value one. Observe that the independent time variable, t, explicitly appears in the BCR4BP pseudo-potential through the Sun terms. Therefore, the BCR4BP is time-dependent and does not admit an integral of the motion. However, a scaled version of the Hamiltonian value in the BCR4BP is defined to be consistent with the Jacobi constant in the CR3BP, i.e.,

$$H(\theta) = 2\Upsilon^* - \left(\dot{x}^2 + \dot{y}^2 + \dot{z}^2\right) \quad [7]$$

Note that the Hamiltonian value is a function of the Sun angle θ and, thus, a function of the independent time variable. Equation [7] relates nondimensional position and velocity states. Thus, similar to

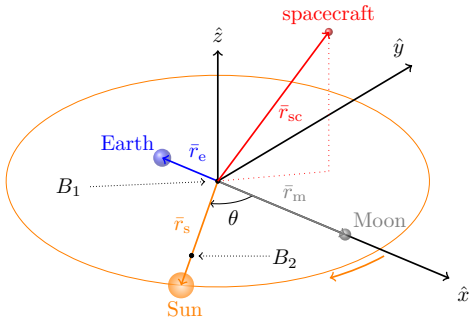

Fig. 1: BCR4BP as formulated in the Earth-Moon rotating frame

the Jacobi constant in the CR3BP, the Hamiltonian, is a nondimensional metric. Equations [4] to [7] describe the Earth-Moon-Sun BCR4BP as defined in the Earth-Moon rotating frame.

In scenarios where the spacecraft departs the Earth-Moon vicinity, its trajectory may be more insightful when represented in the Sun-B_1 rotating frame. The BCR4BP equations of motion are, therefore, also derived in this frame. In the Sun-B_1 rotating frame, the Sun and B_1 are fixed, while the Earth and the Moon are in circular orbits about their barycenter B_1, as illustrated in Fig. 2. The Sun-B_1 rotating frame is centered at B_2. The $\hat{\underline{x}}$-axis is directed from the Sun to B_1, the $\hat{\underline{z}}$ direction is aligned with the Sun-B_1 orbital angular momentum direction, and $\hat{\underline{y}}$ completes the right-handed orthogonal coordinate triad. (Note that underlined variables denote quantities in the Sun-B_1 rotating frame, while non-underlined variables describe quantities as observed in the Earth-Moon rotating frame). In terms of the Sun-B_1 rotating frame, the positions of the Earth and the Moon are uniquely described by the Moon angle, defined as the angle between the rotating $\hat{\underline{x}}$ axis and the position vector from B_1 to Moon, labeled $\bar{\underline{r}}_{B_1\mathrm{m}}$. The equations of motion for the BCR4BP in the Sun-B_1 rotating frame are derived as,

$$\ddot{\underline{x}} = 2\dot{\underline{y}} + \frac{\partial \underline{\Upsilon}^*}{\partial \underline{x}}, \quad \ddot{\underline{y}} = -2\dot{\underline{x}} + \frac{\partial \underline{\Upsilon}^*}{\partial \underline{y}}, \quad \ddot{\underline{z}} = \frac{\partial \underline{\Upsilon}^*}{\partial \underline{z}} \quad [8]$$

where $\underline{\Upsilon}^*$ is the pseudo-potential function defined in the Sun-B_1 rotating frame, i.e.,

$$\underline{\Upsilon}^* = \frac{1}{2}(\underline{x}^2 + \underline{y}^2) + \frac{1 - \frac{1}{\mu_\mathrm{s}+1}}{\underline{r}_{\text{s-sc}}} + \frac{\frac{1}{\mu_\mathrm{s}+1}(1-\mu)}{\bar{\underline{r}}_{\text{e-sc}}} + \frac{\frac{\mu}{\mu_\mathrm{s}+1}}{\underline{r}_{\text{m-sc}}} \quad [9]$$

The equations of motion in the BCR4BP as formulated in the Sun-B_1 rotating frame, in Eq. (8), rep-

resent the same dynamics as the equations of motion for the BCR4BP in the Earth-Moon rotating frame, in Eq. (4).

Consistent with the equations of motion in the CR3BP and the equations of motion for the BCR4BP as formulated in the Earth-Moon rotating frame, the equations of motion describing the BCR4BP dynamics in the Sun-B_1 rotating frame are nondimensionalized. The characteristic quantities include: (i) the Sun-B_1 distance; (ii) the sum of the Sun, Earth and Moon masses; (iii) a characteristic time such that the nondimensional gravitational constant $\tilde{G}$ equals unity. The position of the Earth and the Moon with respect to the system barycenter, B_2, are then defined as,

$$\bar{r}_e = \bar{r}_{B_1} + \bar{r}_{B_1\mathrm{e}} = \begin{bmatrix} 1 - \frac{1}{\mu_s+1} \\ 1 - \frac{1}{\mu_s+1} \\ 0 \end{bmatrix} + \begin{bmatrix} -\frac{\mu}{a_s}\cos(\underline{\theta}) \\ -\frac{\mu}{a_s}\sin(\underline{\theta}) \\ 0 \end{bmatrix}$$

$$\bar{r}_m = \bar{r}_{B_1} + \bar{r}_{B_1\mathrm{m}} = \begin{bmatrix} 1 - \frac{1}{\mu_s+1} \\ 1 - \frac{1}{\mu_s+1} + \\ 0 \end{bmatrix} + \begin{bmatrix} \frac{1-\mu}{a_s}\cos(\underline{\theta}) \\ \frac{1-\mu}{a_s}\sin(\underline{\theta}) \\ 0 \end{bmatrix} \quad [10]$$

where $\underline{\theta} = \pi - \theta = \underline{\omega}t + \underline{\theta}_0$ is the Moon angle, and $\underline{\omega} = \frac{\omega}{1-\omega}$ is the nondimensional angular rate of the Earth and the Moon in their motion around their common barycenter B_1. Alignment of the Sun, Earth, and Moon occurs every synodic period, that is, about 29.5 days. Similar to the BCR4BP formulated in the Earth-Moon rotating frame, the Sun-B_1 BCR4BP is a non-autonomous, periodic system. Consistent with Eq. (7), a scaled Hamiltonian value is defined in the Sun-B_1 rotating frame,

$$\underline{H}(\underline{\theta}) = 2\underline{\Upsilon^*} - \left(\underline{\dot{x}}^2 + \underline{\dot{y}}^2 + \underline{\dot{z}}^2\right) \quad [11]$$

Note that this value is a function of the epoch, i.e., the Moon angle $\underline{\theta}$. The equations of motion for the BCR4BP as viewed in the Earth-Moon frame, in Eq. (4), and the formulation in the Sun-B_1 rotating frame, in Eq. (8), describe the same dynamical system. Thus, trajectory design in the BCR4BP leverages two sets of differential equations, i.e., Eq. (4) and Eq. (8), as well as the rotation matrices to transform states from one frame to the other. The BCR4BP is a versatile dynamical model for trajectory design in the Earth-Moon-Sun multi-body regime.

III. Reference Orbits

A framework is developed to design transfers from the lunar vicinity to heliocentric space. First, a departure baseline orbit, the 9:2 synodic resonant L_2 NRHO, is identified in the lunar vicinity. Then, selected ranges of Sun-B_1 $\underline{L_1}$ and $\underline{L_2}$ halo orbits are leveraged to approximate the flow into and out of the Earth-Moon vicinity. Lastly, maps are constructed to select initial guesses for end-to-end transfers while incorporating energy and phasing considerations.

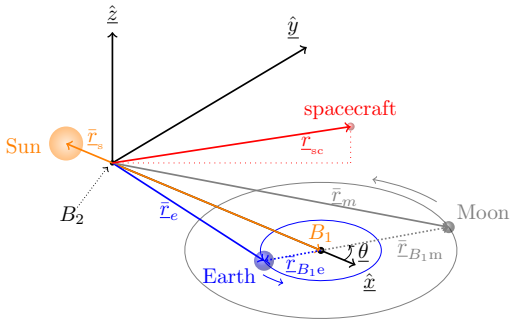

Fig. 2: BCR4BP as formulated in the Sun-B_1 rotating frame

III.i Cislunar Orbits

The selected departure orbit in this investigation is the Earth-Moon 9:2 synodic resonant L_2 NRHO as computed in the BCR4BP. The 9:2 synodic resonant L_2 NRHO is a potential candidate baseline trajectory for a long-term facility near the Moon due its favorable eclipse-avoidance and stability properties[6]. The 9:2 synodic resonant L_2 NRHO as computed in the CR3BP, plotted in black in Figure 3, is transitioned to the BCR4BP using continuation in the Sun mass parameter[7]. Multiple 9:2 NRHOs exist in the BCR4BP[7]; the orbit selected in this investigation is the NRHO that allows

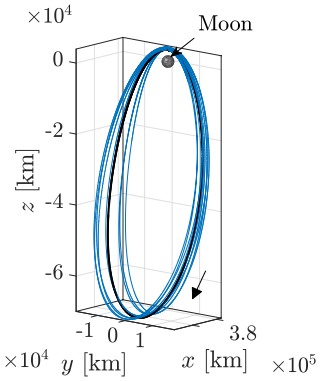

Fig. 3: 9:2 synodic resonant L_2 NRHO in the CR3BP (black) and the BCR4BP (blue)

the largest relative distance with respect to the Earth shadow and is colored in blue in Figure 3. The period of the 9:2 synodic resonant L_2 NRHO in the BCR4BP is equal to exactly two synodic periods, or 9 orbital periods along the 9:2 synodic resonant L_2 NRHO in the CR3BP. The radius ranges corresponding to its nine perilunes (between 3,100 and 3,900 km) and apolunes (between 69,900 and 71,700 km) are consistent with the values of the CR3BP 9:2 synodic resonant L_2 NRHO. The Jacobi constant value remains constant along a periodic orbit in the CR3BP. Its counterpart in the BCR4BP, the Hamiltonian value, varies due to the variation of the Sun angle. For a periodic orbit in the BCR4BP, the Hamiltonian value returns to its initial value after precisely one orbital period. As a potential staging location to various destinations from the lunar vicinity, the 9:2 NRHO as computed in the BCR4BP is selected as the reference departure orbit in this investigation.

III.ii Heliocentric Orbits

Two subsets of the Sun-Earth L_1 and L_2 halo orbit families serve as the baseline Sun-B_1 libration point orbits (LPOs) for this analysis. This investigation focuses on transit to and from Sun-B_1 northern halo orbits that reflect a limited range of z component magnitudes, as plotted in Fig. 4. In addition to a higher associated value of an energy-like quantity, i.e., a lower Jacobi constant in the CR3BP or a lower Hamiltonian value in the BCR4BP, halo orbits with a larger maximum z component magnitude possess a higher inclination relative to the Sun-Earth-Moon plane and are, thus, more challenging to access from the Earth-Moon vicinity.

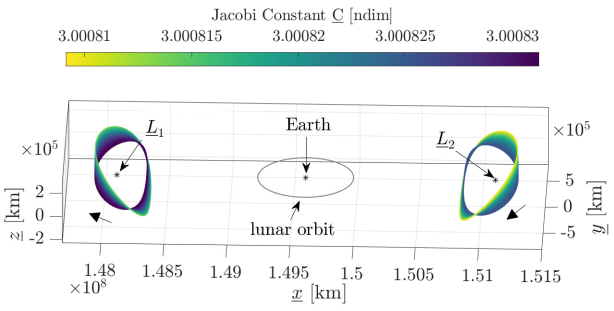

Fig. 4: Representative L_1 and L_2 halo orbits as computed in the CR3BP with maximum z amplitude values between 0 and 250,000 km, colored as a function of the Jacobi constant value

Representative orbits from each of the subsets defined in Fig. 4 are transitioned from the CR3BP to the BCR4BP. An infinite number of periodic solutions, i.e, solutions that precisely repeat in all six position and velocity states over every revolution, exist in the CR3BP[8]. The BCR4BP is formulated to represent a time-dependent, periodic system. Therefore, only isolated periodic orbits with specific orbital periods equal to a multiple of the lunar synodic period exist rather than families with continuously varying periods[9]. Gómez et al.[2] and Boudad[7] use a continuation method to transition synodic resonant orbits from the CR3BP to the BCR4BP. While this approach offers many advantages, it greatly restricts the number of periodic orbits available. Consider the resonance plot in Fig. 5. The horizontal axis represents the maximum z component magnitudes for two subsets of the Sun-B_1 L_1 and L_2 halo families. The vertical axis reflects the synodic resonance ratio, that is, the ratio between the orbital period and the synodic period. The low-amplitude halo orbits of interest for this investigation are highlighted by the green box, and the dashed line identifies the resonance ratio, i.e., one orbital period per six synodic periods. Thus, the halo orbits selected in this investigation evidently do not possess a simple resonance ratio. Note that less intuitive resonance ratios, such as $^{1699}/_{278}$, may be available, but the orbits associated with such resonance ratios usually possess a large number of revolutions and are, therefore, numerically challenging to converge. In the BCR4BP, only isolated, synodic resonant orbits are exactly periodic.

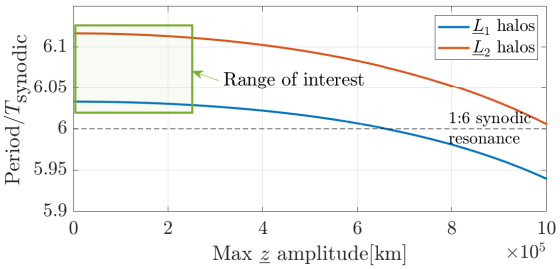

Fig. 5: Synodic resonance ratio plots for a subset of the Sun-B_1 L_1 and L_2 halo families as computed in the CR3BP

To overcome a lack of sufficient synodic resonant orbits in the region of interest, an alternative approach is employed to leverage non-synodic resonant periodic halo orbits. Periodic orbits in the CR3BP are transitioned to reflect simply bounded motion in the BCR4BP. Multiple revolutions of the periodic or-

bit from the CR3BP are 'stacked', discretized, and corrected for continuity in the BCR4BP using a differential corrections scheme and the γ-continuation method[10]. The γ-continuation strategy leverages a parameter, γ, to scale the Earth-Moon distance in the Sun-B_1 rotating frame, allowing continuation from the Sun-B_1 CR3BP to the BCR4BP as formulated in the Sun-B_1 rotating frame. However, periodicity is not enforced: the initial and final states along the corrected trajectory in the BCR4BP do not necessarily match. Bounded motion in the BCR4BP in the vicinity of a CR3BP $\underline{L}_2$ halo orbit is plotted in Figure 6. The $\underline{L}_2$ equilibrium point and its instantaneous $\underline{E}_2$ counterparts in the BCR4BP are denoted by red dots and are indistinguishable at this scale. The BCR4BP set of instantaneous equilibrium points is the collection of points with a value of rotating velocity and acceleration that is instantaneously zero for a given Sun angle[4]. Thirty revolutions, or approximately 15 years, of bounded motion near the CR3BP halo orbit are produced in the BCR4BP, and viewed in Fig. 6. Note that the halo orbits leveraged in this investigation are linearly unstable[10], thus, discretization of the trajectory and a numerical corrections scheme are necessary to produce these long, bounded trajectories.

IV. Transfer Framework

The round-trip transfer design problem from an Earth-Moon NRHO to/from a Sun-B_1 halo orbit is introduced. A flowchart detailing the different phases of the transfer construction procedure, and the free/fixed parameters along each phase is summarized. Unstable and stable manifolds from the heliocentric halo orbit are propagated forward and backward in time, respectively, and trajectories that encounter a close perilune in the Earth-Moon system are recorded. Families of transfer trajectories originating or terminating at a close perilune state are then produced and summarized in maps. The perilune transfers maps extend the pool of potential initial guesses that are leveraged to construct the end-to-end, round-trip transfers between cislunar and heliocentric spaces.

IV.i Problem Formulation

With the upcoming James Webb Space Telescope and the Nancy Roman Space Telescope, opportunities for servicing missions between cislunar space and heliocentric space will arise in the near future. In this investigation, the round-trip servicing trajectories are required to originate and end in the Earth-Moon 9:2 NRHO. Recall that the 9:2 synodic resonant L_2 NRHO is the candidate baseline orbit for the Gateway facility[6] and is intended to serve as a stepping location to destinations beyond the Earth-Moon vicinity. The intermediate destination for the round-trip trajectory is a $\underline{L}_1$ or $\underline{L}_2$ Sun-B_1 halo orbit. A flowchart detailing the phases of the trajectory construction procedure appears in Fig. 7. The trajectory arc from the Earth-Moon NRHO to the Sun-B_1 halo orbit is denoted the 'outbound leg', while the arc from the heliocentric halo to the 9:2 synodic resonant L_2 NRHO is labeled the 'inbound leg'.

The parameters along each phase of the transfer are detailed. The phasing of the cislunar orbit, that is, the 9:2 synodic resonant L_2 NRHO, is fixed for both the outbound and inbound parts of the transfer. Consistent with the baseline NRHO for the Gate-

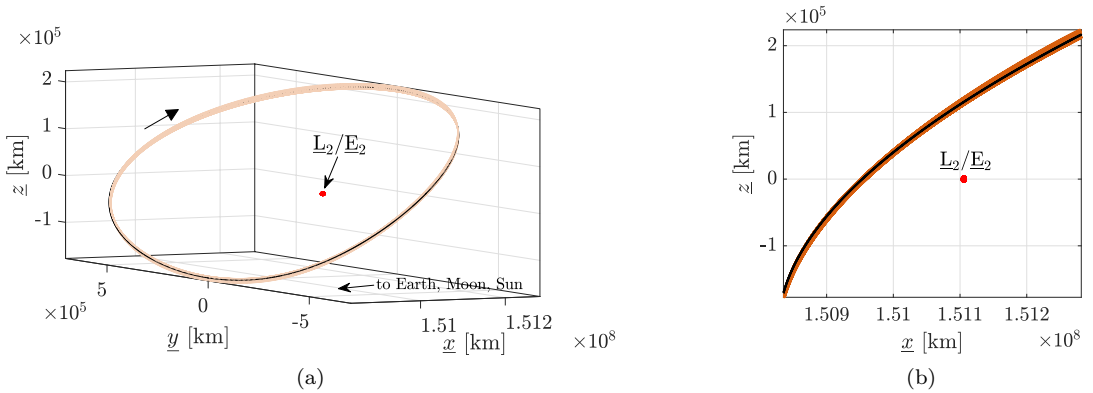

Fig. 6: Isometric (a) and side (b) views of the bounded BCR4BP motion (in orange) in the vicinity of the $\underline{L}_2$ CR3BP halo orbit (in black) with max. $\underline{z}$ amplitude equal to 125,000 km

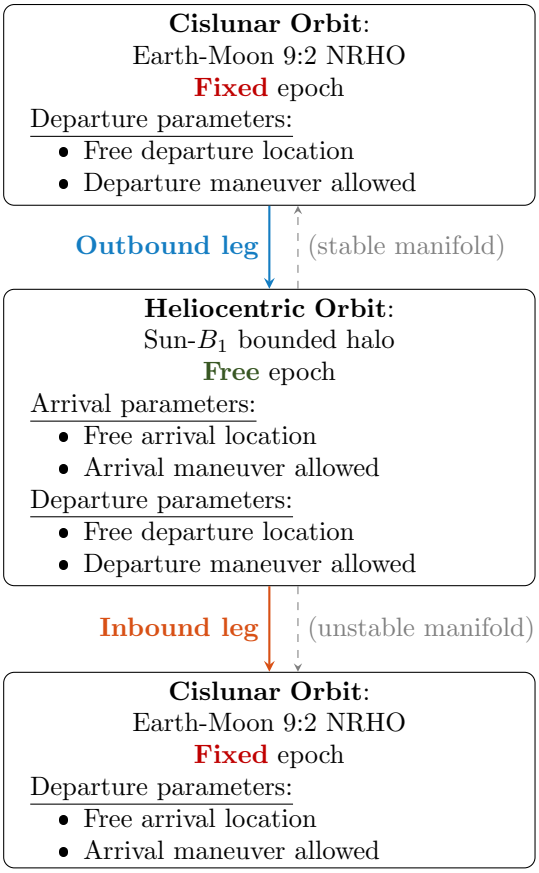

Fig. 7: Flowchart for the round-trip trajectory design framework. Fixed and free parameters along each of part of the transfer are labeled. The underlying natural motion for each leg is identified in gray.

way facility, the phase of the 9:2 NRHO is selected such that the distance to the Earth shadow is maximized, providing an entirely Earth eclipse-free trajectory. By fixing the phase of the NRHO for both the outbound and inbound legs, returning to the same phase as the Gateway vehicle facilitates an eventual rendezvous after arrival. The departure and arrival locations along the NRHO are free variables in the design process. However, it is necessary that certain regions likely are excluded, such as the region near perilune due to the high relative velocity magnitudes with respect to the Moon. The phasing of the Sun-B_1 halo orbit is free in the initial development of the design process. Allowing the phasing and thus, the epoch, of the heliocentric orbit to vary increases the number of potential connections between heliocentric arcs and the lunar vicinity. The phasing of the heliocentric orbit may be eventually be constrained if the objective is a rendezvous with an object, for instance, a specific solar observatory or space telescope in orbit. Similarly to the cislunar orbit, the departure and arrival locations are free. The options for the maneuvers are noted in Fig. 7: maneuvers are allowed for departure and arrival along both the cislunar and heliocentric orbits. Finally, the grey dashed arrows in the figure details the underlying natural motions that are leveraged for the initial guess generation.

IV.ii Initial Guess Generation

Transfers leveraging the natural dynamics to and from the heliocentric orbits are sought. Thus, manifolds associated with the Sun-B_1 halo orbits are incorporated. Manifolds reflect the local ballistic flow approaching and departing an unstable periodic orbit and are frequently exploited for transfer design [11,12]. While multiple metrics are available to measure stability, such as various types of indices [13,14], the stability (in the linear sense) of a periodic solution is assessed here using the Lyapunov exponent ϕ [7], that is,

$$\phi_i = \Re\left(\frac{\ln \lambda_i}{\mathbb{P}}\right) \qquad [12]$$

where λ_i is the i-th eigenvalue from the monodromy matrix, that is, the state-transition matrix computed for one orbital period, $\mathbb{P}$. The necessary condition for linear stability of a periodic orbit is that all the Lyapunov exponents must be equal to zero. One or more nonzero Lyapunov exponents denote instability and, thus, the existence of approaching and departing flows with respect to the orbit. The stability characteristics for the two subsets of the Sun-B_1 $\underline{L}_1$ and the $\underline{L}_2$ halo orbits are initially explored. All the orbits across both subsets as seen in Fig. 4 possess one unstable mode; the range of the Lyapunov exponents for each unstable mode is summarized in Table 1. Note the similar range for the Lyapunov exponents in the two subsets. Thus, approaching and departing flows from the selected orbits possess similar arrival and departure rates.

Table 1: Stability information associated with the Sun-B_1 CR3BP $\underline{L}_1$ and $\underline{L}_2$ halo orbits with maximum $\underline{z}$ component magnitude between 0 and 250,000 km

Subset	Unstable mode(s)	Range of ϕ_i for the unstable mode(s)
$\underline{L}_1$ halo	1	$\pm 2.4207 - \pm 2.4431$
$\underline{L}_2$ halo	1	$\pm 2.3757 - \pm 2.3961$

The bounded motions in the BCR4BP correspond-

ing to the non-synodic resonant CR3BP orbits are, by definition, not periodic. Thus, there is no monodromy matrix associated with a bounded motion, and the Lyapunov exponent for the entire time-of-flight associated with a multi-revolution baseline may not be an insightful metric. However, subsequent revolutions along a bounded BCR4BP solution tend to remain close to each other, as apparent in Fig. 6. Thus, an approximate monodromy matrix is computed for each quasi-revolution along the bounded motion, and approximate unstable and stable directions are produced. These approximate manifold directions provide adequate estimates for departing and approaching the heliocentric halo orbits for the purpose of this investigation. Note that directions other than the (approximate) unstable and stable directions, such as the maximum stretching and restoring directions[15], may offer alternative directions for the flow departing and approaching the heliocentric orbit. Approximate stable and unstable manifold directions are employed in this investigation for leveraging the natural arcs to and from the Sun-B_1 halo orbits.

Consider the process for the generation of an initial guess for the outbound leg, that is, the Earth-Moon NRHO to Sun-B_1 halo orbit transfer as defined in Fig. 7. This process leverages the stable manifold of the Sun-B_1 orbit and backwards propagation. A similar strategy is employed for generating an initial guess for the inbound leg but employs the unstable manifold of the heliocentric orbit and forward propagation. The BCR4BP bounded motions, corresponding to representative Sun-B_1 CR3BP halo orbits from Fig. 4, are discretized and trajectories along the approximate stable manifold path are propagated. As these trajectories evolve toward the Earth (when propagated in negative time), a small subset of the arcs encounters the Moon. A sample of these trajectories for the heliocentric orbits on the $\underline{L}_1$ side appears in Fig. 8. A perilune within 30,000 km of the Moon, denoted by a colored dot in Fig. 8, occurs along each of these trajectories. The color of the lines denote the $\underline{z}$ component magnitude of a destination orbit from among the subset of options; the out-of-plane nature of these trajectories is apparent in Fig. 8(b). In general, multiple geometries for transfer trajectories between heliocentric orbits and the lunar vicinity are efficiently produced from back- or forward-propagation of the manifolds associated with the Sun-B_1 halo orbit.

Families of transfers to (respectively, from) the Sun-B_1 halo orbits from (respectively, to) the lunar region are constructed using favorable trajectories along the approximate manifolds of the halo orbits. These families of perilune transfer trajectories increase the number of potential initial guesses for end-to-end, round trip transfers between the Earth-Moon 9:2 synodic resonant L_2 NRHO and the Sun-B_1 heliocentric halo orbit. For each member of the family, the departure state is constrained as a perilune, and an insertion maneuver into the Sun-B_1 halo orbit is allowed. (For transfers *from* the heliocentric orbit, the arrival state is constrained as a perilune and a departure maneuver from the Sun-B_1 halo is allowed.) Employing a continuation process, families of transfers are then produced in two continuation parameters: departure perilune radius and time-of-flight. As an illustration, consider the perilune transfer family to a BCR4BP bounded halo with 125,000

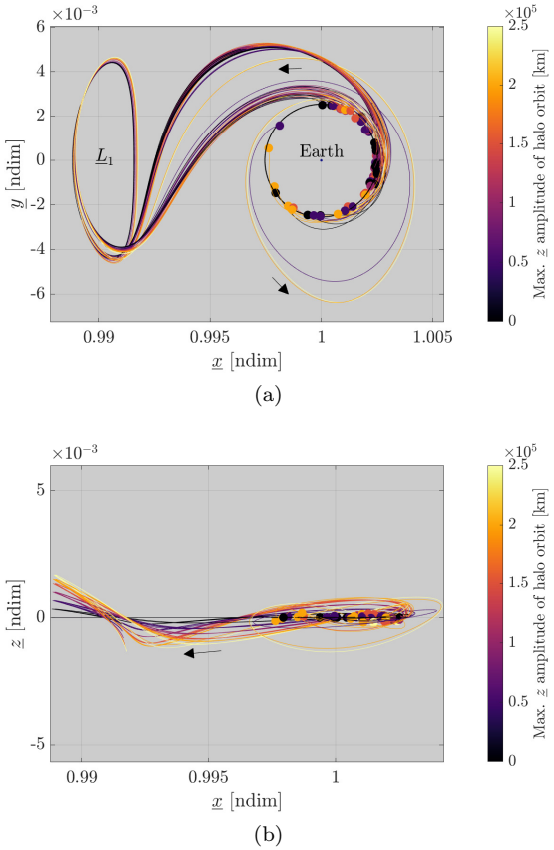

Fig. 8: Trajectories along the approximate stable manifold for a various range of Sun-B_1 $\underline{L}_1$ halo bounded motion, as computed in the BCR4BP. All the trajectories encounter a perilune within 30,000 km of the Moon; the perilunes are denoted by colored dots.

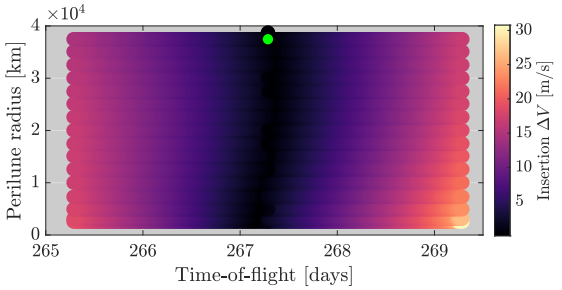

Fig. 9: Map of transfers from perilune states to the $\underline{L}_2$ halo bounded motion with 125,000 km maximum $\underline{z}$ component magnitude, as computed in the BCR4BP. The initial guess from the approximate manifold are is denoted by a green dot.

km maximum $\underline{z}$ component magnitude in Fig. 9. The horizontal axis represents the time of flight between the departure state at perilune and the insertion maneuver at the Sun-B_1 orbit. The vertical axis corresponds to the radius from the Moon to the perilune departure state. Each dot corresponds to a converged transfer and is colored by the insertion ΔV cost. The initial guess from the stable manifold arc associated with the destination halo orbit is plotted as a green dot. Two steps are employed to continue this transfer into families of feasible transfer options. First, the time of flight is maintained as tired while the family of transfers is continued in terms of perilune radius. This first family of transfers corresponds to the vertical line in Fig. 9. Then, families of transfers are continued off this first solution set. For various selected perilune radii, the corresponding converged transfers in the first family are continued in time of flight, corresponding to the horizontal lines in Fig. 9. Using this two-step continuation process, transfers are produced for departure perilune states with lunar radii between 3,000 km and 40,000 km, and the times-of-flight range from 265 to 270 days. Most of the transfers to the selected heliocentric halo orbit require an insertion ΔV maneuver of less than 20 m/s. The availability of the perilune transfers map increases the number of potential initial guesses for the end-to-end, cislunar-to-heliocentric trajectory design.

Initial guesses for the end-to-end transfers are selected from the map of perilune transfers, in Fig. 9, over a set of certain parameters. Boudad et al.[10,16] identify the energy and phasing parameters of interest to seed an initial guess for an end-to-end transfer. A numerical scheme to implement the differential corrections process is employed to produce continuous round-trip BCR4BP transfers between the Earth-Moon NRHO and the selected Sun-B_1 halo orbit. In this investigation, the differential corrections schemes for the map generation and the transfer construction are applied to states as represented in the Sun-B_1 rotating frame. However, recall that the dynamics in the BCR4BP as described by the equations of motion in the Earth-Moon rotating frame (Eqs. (4) and (5)) are identical to the behavior modeled by the equations of motion in the Sun-B_1 frame (Eqs. (8) and (9)). Thus, numerical corrections could also be employed on states represented in the Earth-Moon rotating frame[17]. The initial guess trajectory is discretized into patch points to facilitate the convergence process. While a single-shooting algorithm is an acceptable alternative in certain scenarios, it generally fails for long transfers with close passages of one or more primaries. The transfers in this investigation are characterized by times-of-flight of over a year, and one or more close (less than 30,000 km) approaches to the Moon. Thus, a multiple-shooting scheme is selected for the numerical corrections algorithm. The trajectory is corrected for continuity between consecutive patch point arcs. Maneuvers are allowed at the departure and arrival locations along each orbit, that is, at departure and arrival in the Earth-Moon 9:2 synodic resonant L_2 NRHO and in the Sun-B_1 halo orbit. The time of flight is not explicitly allowed to vary during the corrections process, but is adjusted by modifying the departure location along the Earth-Moon NRHO. Recall that the BCR4BP is a time-dependent, periodic model. Thus, adjusting the departure state also changes the departure time and, thus, modifies the time of flight. Once a transfer satisfies the constraints within some numerical tolerance, families of transfers are produced by continuing the numerical corrections along some parameter, such as departure or arrival locations from the NRHO.

V. Results

A sampling of round-trip transfer families to heliocentric orbits near the $\underline{L}_1$ and $\underline{L}_2$ Lagrange points are examined. To construct a families of inbound or outbound transfers, an initial guess is first select along a perilune transfers map as viewed in Fig. 9. The time-of-flight along this initial guess is adjusted to be continuous in epoch with the selected departure or arrival state along the 9:2 synodic resonant L_2 NRHO. In cases where the epoch discontinuity between the initial guess and the NRHO state is significant, additional trajectory arcs, labelled 'bridge arcs',

are employed to facilitate the process. A numerical differential corrections scheme on the transfer trajectory is then employed to reduce the discontinuities between consecutive patch points to within a specified tolerance, while allowing the maneuvers noted in Fig. 7. Once a continuous end-to-end transfer is obtained, it may be continued into a family of transfers by varying a parameter, such as the maneuver location and repeating the differential corrections process. Among the constructed families of outbound and inbound transfers, a round-trip trajectory that presents the lowest ΔV for each leg and its characteristics are explored.

V.i Round-trip Transfers to Sun-Earth $\underline{L}_1$ Orbits

Families of end-to-end outbound and inbound transfers between the 9:2 synodic resonant L_2 NRHO and the Sun-B_1 halo orbits around the $\underline{L}_1$ libration point are constructed. As an illustration, consider the transfer families to and from the BCR4BP $\underline{L}_1$ halo bounded motion with maximum $\underline{z}$ component magnitude equal to 225,000 km, as produced in Fig. 10. Two families are plotted in each figure: one corresponding to the inbound transfers and one for the outbound transfers. Each arc is colored as a function of the total ΔV along the leg. For instance, the total ΔV along the outbound leg is the sum of the departure maneuver from the Earth-Moon NRHO and the arrival maneuver into the Sun-B_1 halo orbit. The transfer families in Fig. 10 possess a total leg ΔV ranging between 98 and 300 m/s for the outbound family, and ranging between 245 and 300 m/s. (The maximum allowable ΔV magnitude for one leg of the round trip was set to 300 m/s in this analysis). The times-of-flight range from 220 to 226 days for the outbound transfers, and from 254 to 257 days for the inbound legs. The geometry of the transfers with respect to the Sun-B_1 rotating frame is apparent in Fig. 10(a). The cislunar and heliocentric orbits are colored in blue and the lunar orbit is the gray circle. The location of the CR3BP libration point and its osculating BCR4BP counterparts are denoted by the green points, and are indistinguishable at this scale. The maneuver locations along the NRHO are highlighted by white dots. The geometry of the transfers near the Moon, as viewed in the Earth-Moon rotating frame, is also explored in Fig. 10(b). The locations for the NRHO departure and arrival maneuvers occur near an apolune, but on different revolutions along the NRHO. Note that no departure or arrival location is selected close to perilune: near this apse, higher dynamical sensitivities introduce different challenges in constructing consistent transfers and, thus, are avoided. The outbound and inbound transfer families both include additional revolutions around the Moon near the NRHO after departure and before arrival, respectively. The geometry of these extra revolutions suggest some arcs from a higher-period dynamical structures[13] are possibly leveraged to access and depart from the vicinity of the NRHO.

The round-trip transfer from the Earth-Moon 9:2 synodic resonant L_2 NRHO to the selected Sun-B_1 halo orbit that reflects the lowest total ΔV cost is plotted in Fig. 11. The associated total time-of-flight is 616 days and the total ΔV cost is 412 m/s. For

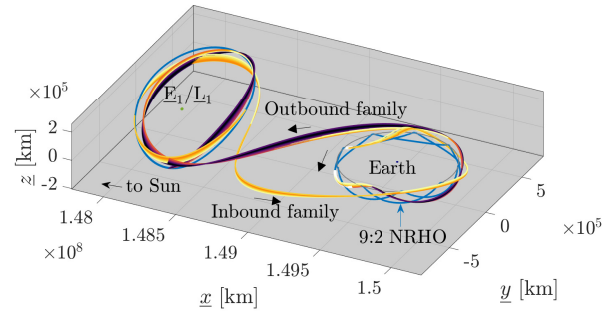

(a) Sun-B_1 rotating frame

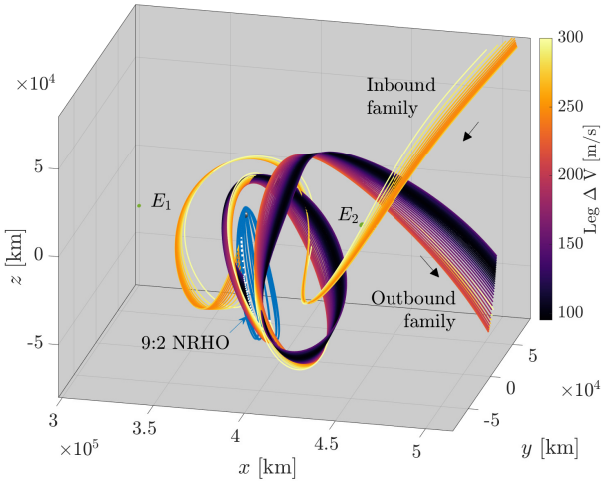

(b) Earth-Moon rotating frame

Fig. 10: Outbound and inbound transfers as computed in the BCR4BP. The heliocentric orbit is the $\underline{L}_1$ halo bounded motion with 225,000 km maximum $\underline{z}$ component magnitude.

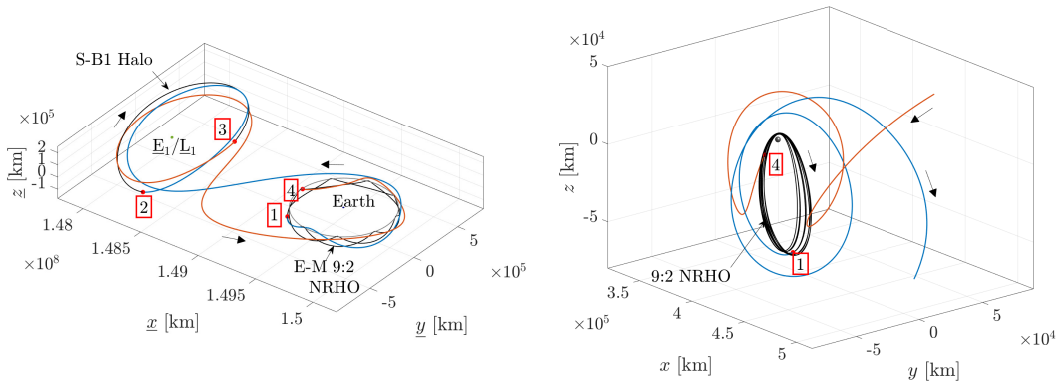

(a) Sun-B_1 rotating frame (b) Earth-Moon rotating frame

Fig. 11: Round-trip transfer with the lowest total ΔV cost among the transfers in Fig. 10. The total ΔV is 412 m/s and the total time-of-flight is 616 days.

a round-trip transfer, the time-of-flight is defined as the sum of the time-of-flight along the outbound leg, the time spent in the heliocentric halo orbit, and the time-of-flight on the inbound leg. The location of the maneuvers is highlighted by red dots and text boxes in Fig. 11; all four maneuvers are apparent in the Sun-B_1 rotating frame in Fig. 11(a). The initial and final maneuvers along the transfer, i.e., the departure from and insertion into the Earth-Moon NRHO are visible in Fig. 11(b). The magnitudes of each the maneuvers is listed in Table 2. The majority (approximately 65%) of the total ΔV cost is employed for the insertion into the Earth-Moon NRHO on the inbound leg of the transfer. This high insertion cost could potentially be reduced using a different initial guess for the inbound leg. Despite this relatively high insertion ΔV maneuver magnitude, note that natural Sun-Earth-Moon dynamical flow is leveraged for the round-trip transfer. Consider the Sun-B_1 rotating velocity profile along the round-trip transfer as a function of the time along the trajectory in Fig. 12. The colors are consistent with Fig. 11: black for the cislunar and heliocentric orbits, blue for the outbound leg and orange for the inbound leg. The black spikes correspond to the rapid velocity change near perilune along the Earth-Moon 9:2 NRHO. Small discontinuities are apparent at each color transition; each discontinuity corresponds to a ΔV maneuver and is identified by a red label. The small, sometimes indistinguishable, discontinuities do not significantly change the post-maneuver evolution of the velocity curve. Therefore, the round-trip transfer between the Earth-Moon NRHO and the Sun-B_1 libration point orbit leverages the natural Sun-Earth-Moon dynamical flow.

Table 2: ΔV maneuvers along the round-trip transfer in Fig. 11

Maneuver	Label	Magnitude [m/s]
E-M NRHO departure	1	77.3
S-B1 halo arrival	2	20.6
S-B1 halo departure	3	43.1
E-M NRHO arrival	4	271.5
Total		**412.4**

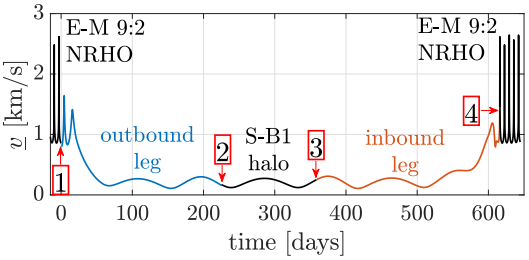

Fig. 12: Sun-B_1 rotating velocity profile as a function of the time along the round-trip transfer in Fig. 11

V.ii Round-trip Transfers to Sun-Earth $\underline{L}_2$ Orbits

Using this trajectory design framework, families of round-trip BCR4BP transfers to the Sun-B_1 $\underline{L}_2$ halo orbits are also successfully constructed. For example, consider the trajectories in Fig. 13. The selected halo bounded motion has a maximum $\underline{z}$ component magnitude equal to 185,000 km. Recall that the cislunar orbit is the 9:2 synodic resonant L_2 NRHO with a phase consistent with the Gateway baseline orbit. Similar to the transfers in Fig. 10, the trajectories are colored as a function of the ΔV along each leg. A round-trip transfer involves an outbound (NRHO to Halo) leg and an inbound (Halo to NRHO) leg. Thus, the total ΔV for a round-trip transfer is the sum of the ΔV's for each leg. The ΔV for the transfers along the family in Fig. 13 range from 144 to 255 m/s for the outbound transfers and from 178 to 255 m/s for the inbound legs. The time-of-flight varies between 232 and 236 days, and between 307 and 312 days for the outbound and inbound trajectories, respectively. The times-of-flight between outbound and inbound legs may differ for a variety of reasons. First, the departure/arrival motion from the Sun-B_1 LPO leverages the approximate manifold associated with the orbit. Thus, the spacecraft may be in close proximity to the heliocentric orbit over a significant amount of time before the insertion maneuver (in the case of the outbound trajectories) and the end of the transfer leg. This 'winding' onto the LPO, apparent in Fig. 13(a), is generally different for the outbound and inbound transfers and thus, results in different ranges for times-of-flight for the two parts of the transfer. Second, the geometry of the outbound and inbound transfers themselves are in general different. There is no resonance between the Earth-Moon 9:2 synodic resonant L_2 NRHO and the range of Sun-B_1 LPOs in Fig. 4 that can be exploited in this investigation. If a resonance exists, symmetric, repeatable round-trip transfers would be available between the Earth-Moon NRHO and the Sun-B_1 halo orbit. Since it is not the case here, the geometries and, thus, the times-of-flight for the outbound and inbound legs differ to accommodate the change in relative phasing between the two orbits. Note the additional lobe and apogee along the inbound transfers as viewed in the Sun-B_1 rotating frame in Fig. 13. This geometry is similar to the one associated with ballistic lunar transfers [18]. Inbound and outbound transfers that possess different Sun-B_1 geometries and times-of-flight are constructed in the BCR4BP employing the proposed trajectory design framework.

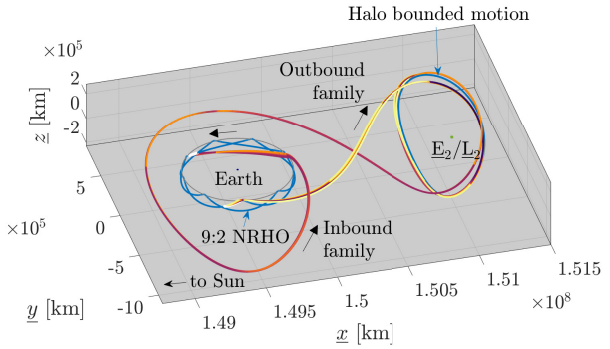

(a) Sun-B_1 rotating frame

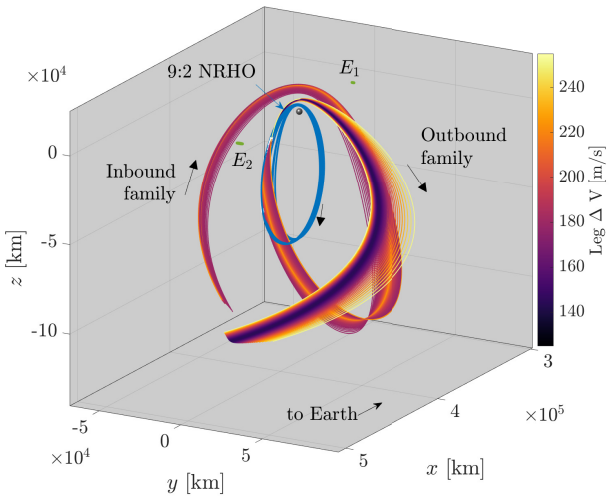

(b) Earth-Moon rotating frame

Fig. 13: Families of outbound and inbound transfers, as computed in the BCR4BP. The heliocentric orbit is the $\underline{L}_2$ halo bounded motion with 185,000 km maximum $\underline{z}$ component magnitude.

The transfers are also examined in the vicinity of the NRHO, in the Earth-Moon rotating frame, as plotted in Fig. 13(b). In contrast to the transfers in Fig. 10, these transfers do not possess multiple revolutions near the NRHO after departure or before arrival. In Fig. 13, the outbound trajectories directly depart the vicinity of the NRHO after the departure maneuver; the inbound trajectories present one large revolution near the NRHO before the insertion ΔV maneuver. The location of the maneuvers along the NRHO are denoted by the white dots. Both departure and arrival maneuvers occur after an apolune state, that is, on the side of the NRHO with a negative rotating $\underline{y}$ component. Note that such as a location is not a requirement for constructing trans-

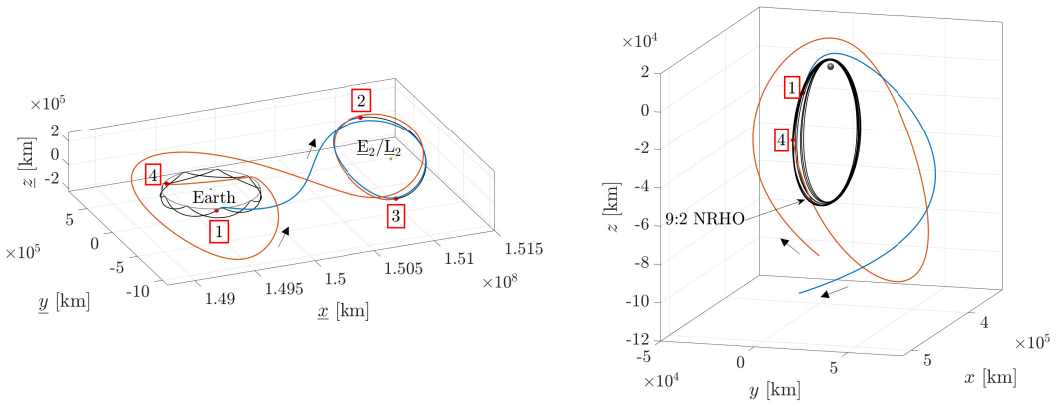

(a) Sun-B_1 rotating frame (b) Earth-Moon rotating frame

Fig. 14: Round-trip transfer with the lowest total ΔV cost among the transfers in Fig. 13. The total ΔV is 323 m/s and the total time-of-flight is 638 days.

fers: transfer families departing (or arriving) to a state prior to an apolune have been successfully constructed using this framework [16].

The round-trip transfer from the Earth-Moon NRHO to the Sun-Earth L_2 LPO that offers the lowest total ΔV cost is extracted from Fig. 13 and plotted in Fig. 14. The color along each arc is consistent with Fig. 7 and each maneuver is located by a red dot and a label. Note that only the initial and final maneuvers are visible in the Earth-Moon rotating frame view in Fig. 14(b). The total ΔV value associated with this transfer is 323 m/s and the associated time-of-flight is 638 days. Recall that the time-of-flight along a round-trip is comprised of the times-of-flight along the outbound and inbound legs, as well as the time-of-flight along the heliocentric LPO, between the arrival and departure maneuvers. The magnitude for each of the four maneuvers along the transfer is summarized in Table 3.

Table 3: ΔV maneuvers along the round-trip transfer in Fig. 14

Maneuver	Label	Magnitude [m/s]
E-M NRHO departure	1	124.5
S-B1 halo arrival	2	19.8
S-B1 halo departure	3	23.6
E-M NRHO arrival	4	155.2
Total		**323.1**

As compared to the transfer to the L_1 region in Figs. 11 and 12, the ΔV budget is relatively balanced between the two parts of the transfers. The ΔV cost for the outbound leg (i.e., maneuvers 1 and 2) is 144.3 m/s while the maneuvers (3 and 4) for the inbound leg amount to 179 m/s. The Sun-B_1 rotating velocity profile along the transfer is presented as a function of time along the trajectory in Fig. 15. The small discontinuities at each color transition represents the ΔV maneuver and is indicated by a red arrow and label. Similar to the velocity profile for the round-trip transfer to the L_1 LPO in Fig. 12, the velocity profile in Fig. 15 is nearly continuous; the maneuvers do not significantly affect the downstream evolution of the velocity profile. Thus, the round-trip transfer that is constructed between the Earth-Moon 9:2 synodic resonant L_2 NRHO and the selected heliocentric L_2 LPO leverages the natural dynamics of the blended Earth-Moon-Sun system.

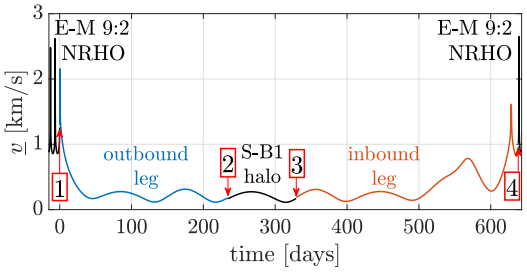

Fig. 15: Sun-B_1 rotating velocity profile as a function of the time along the round-trip transfer in Fig. 14

VI. Concluding Remarks

Many opportunities for regular transit between the lunar vicinity and heliocentric orbits will arise in the near future. Such scenarios include servicing missions to space telescopes such as the James Webb Space Telescope and the Nancy Roman Space Telescope, departure to destinations beyond the Earth-Moon vicinity, as well as safe disposal of various objects. This investigation extends a framework for designing such transfers within the Earth-Moon-Sun BCR4BP. The BCR4BP is a time-dependent, periodic model that incorporates the gravitational influences of the Earth, the Moon, and the Sun, acting on a spacecraft. Transfer design within the BCR4BP blends natural flow from both the Earth-Moon and the Sun-Earth systems. One advantage of the BCR4BP is that relevant information concerning the trajectory is available in two frames: the Earth-Moon rotating frame and the Sun-Earth rotating frame. Yet, the BCR4BP avoids the added complexity of the higher-fidelity force model while the dynamics of the Earth-Moon-Sun system are described relatively accurately.

The cislunar and heliocentric orbits are defined within the context of the Earth-Moon-Sun BCR4BP. The cislunar orbit is selected as the Gateway facility baseline orbit, that is, the Earth-Moon synodic resonant Near Rectilinear Halo Orbit (NRHO). As a synodic resonant orbit, the 9:2 NRHO is transitioned to a precisely periodic orbit in the BCR4BP. The heliocentric orbits are defined as Sun-B_1 $\underline{\mathrm{L}}_1$ and $\underline{\mathrm{L}}_2$ halo Libration Point Orbits (LPOs). To overcome the lack of sufficient resonant LPOs in the region of interest, an alternative approach is employed to leverage non-synodic resonant halo orbits. Employing this approach, bounded multi-year baseline trajectories are constructed in the BCR4BP for a variety of Sun-Earth halo orbits on both the Sun-B_1 $\underline{\mathrm{L}}_1$ and $\underline{\mathrm{L}}_2$ sides.

A transfer framework is described. Natural motion to and from the lunar vicinity is explored using an approximate manifold from the BCR4BP halo orbits. As these trajectories evolve towards the Moon (for the trajectories along the approximate unstable manifold), a small subset of the arcs encounters the Moon. These ballistic arcs represent natural pathways in the Sun-Earth-Moon system and are leveraged to build perilune transfer families. The perilune transfer families extend the pool of available initial guesses for the end-to-end transfer between the Earth-Moon NRHO and the Sun-B_1 LPO, and are summarized in perilune transfer maps. An initial guess selected from a perilune transfer map is then corrected using a differential corrections scheme, resulting in a continuous end-to-end trajectory.

To illustrate the trajectory design framework, multiple families of round-trip transfers between the Earth-Moon 9:2 synodic resonant BCR4BP NRHO and $\underline{\mathrm{L}}_1/\underline{\mathrm{L}}_2$ halo LPOs are constructed. The transfers represent a range of departure and arrival epochs along the Earth-Moon NRHO, as well as a variety of the geometries near the Moon and in heliocentric space. Round-trip transfers offering low total ΔV magnitude are extracted from the transfer families and explored. The proposed trajectory design framework is successfully employed to design round-trip transfers between the Gateway facility orbit and heliocentric space, while overcoming the challenges in the phasing and energy discrepancies associated with problems involving of blended dynamical systems.

Acknowledgements

This work was conducted at Purdue University and NASA Johnson Space Center. The authors thank members of the Multibody Dynamics Research Group at Purdue University for useful discussions. Also acknowledged is the Purdue University School of Aeronautics and Astronautics for facilities and support, including access to the Rune and Barbara Eliasen Visualization Laboratory. This work was supported by a Purdue Bilsland Dissertation Fellowship and NASA Contract NNJ13HA01C with additional effort under NASA grant 80NSSC18M0122.

References

[1] V. G. Szebehely. *Theory of Orbits, the Restricted Problem of Three Bodies*. Academic Press, 1967.

[2] G. Gómez, J. Llibre, R. Martínez, and C. Simó. *Dynamics And Mission Design Near Libration Points - Vol II: Fundamentals: The Case Of Triangular Libration Points*. World Scientific Monograph Series In Mathematics. World Scientific Publishing Company, 2001.

[3] M. Jorba-Cuscó, A. Farrés, and A. Jorba. Two Periodic Models for the Earth-Moon System. *Frontiers in Applied Mathematics and Statistics*, 4:32, 2018.

[4] K. K. Boudad. *Disposal Dynamics From The Vicinity Of Near Rectilinear Halo Orbits In The Earth-Moon-Sun System*. M.S. Thesis, Purdue University, West Lafayette, Indiana, 2018.

[5] E. M. Zimovan, K. C. Howell, and D. C. Davis. Near Rectilinear Halo Orbits and their Application in Cis-Lunar Space. In *3rd International*

Academy of Astronautics Conference on Dynamics and Control of Space Systems, Moscow, Russia, 2017.

[6] D. E. Lee. White Paper: Gateway Destination Orbit Model: A Continuous 15 Year NRHO Reference Trajectory. Technical report, NASA, 2019.

[7] K. K. Boudad, K. C. Howell, and D. C. Davis. Dynamics of Synodic Resonant Near Rectilinear Halo Orbits in the Bicircular Four-Body Problem. *Advances in Space Research*, 66(9):2194–2214, November 2020.

[8] K. C. Howell. Families of Orbits in the Vicinity of the Collinear Libration Points. *Journal of the Astronautical Sciences*, 49, 1998.

[9] R. A. Broucke. Stability of Periodic Orbits in the Elliptic, Restricted Three-Body Problem. *AIAA Journal*, 1969.

[10] K. K. Boudad, K. C. Howell, and D. C. Davis. Heliocentric Access from Cislunar Space within the Context of the Bicircular Restricted Four-Body Problem. In *AAS/AIAA Astrodynamics Specialist Conference*, Lake Tahoe, California (Virtual), August 2020.

[11] W. Koon, M. Lo, J. Marsden, and S. Ross. *Dynamical Systems, the Three-Body Problem and Space Mission Design*. Interdisciplinary Applied Mathematics. Springer New York, 2006. ISBN 9780387564678.

[12] M. Kakoi. *Design of Transfers from Earth-Moon L1/L2 libration point orbits to a destination object*. M.S. Thesis, Purdue University, West Lafayette, Indiana, 2015.

[13] E. M. Zimovan-Spreen, K. C. Howell, and D. C. Davis. Near Rectilinear Halo Orbits and Nearby Higher-Period Dynamical Structures: Orbital Stability and Resonance Properties. *Celestial Mechanics and Dynamical Astronomy*, 2020.

[14] N. Bosanac. *Exploring the Influence of a Three-Body Interaction Added to the Gravitational Potential Function in the Circular Restricted Three-Body Problem: a Numerical Frequency Analysys*. M.S. Thesis, Purdue University, 2012.

[15] V. Muralidharan. *Stretching Directions In Cislunar Space: Stationkeeping and an Application to Transfer Trajectory Design*. Ph.D. dissertation, Purdue University, West Lafayette, Indiana, 2021.

[16] K. K. Boudad, K. C. Howell, and D. C. Davis. Energy and Phasing Considerations for Low-Energy Transfers from Cislunar to Heliocentric Space. In *31st AAS/AIAA Spaceflight Mechanics Meeting*, Charlotte, North Carolina (Virtual), February 2021.

[17] S. T. Scheuerle, B. P. McCarthy, and K. C. Howell. Construction of Ballistic Lunar Transfers Leveraging Dynamical Systems Techniques. In *AAS/AIAA Astrodynamics Specialist Conference*, Lake Tahoe, California, 2020.

[18] J. Parker and R. Anderson. *Low-Energy Lunar Trajectory Design*. JPL Deep-Space Communications and Navigation Series. Wiley, 2014. ISBN 9781118853870.